Journal of Power Sources 196 (2011) 4019–4025

Contents lists available at ScienceDirect

Journal of Power Sources

journal homepage: www.elsevier.com/locate/jpowsour

Preparation of silver-modified $La_{0.6}Ca_{0.4}CoO_3$ binary electrocatalyst for bi-functional air electrodes in alkaline medium

Shuxin Zhuang, Kelong Huang*, Chenghuan Huang, Hongxia Huang, Suqin Liu, Min Fan

College of Chemistry and Chemical Engineering, Central South University, Yuelu Road, Changsha, Hunan 410083, China

ARTICLE INFO

Article history:
Received 18 May 2010
Received in revised form 5 November 2010
Accepted 9 November 2010
Available online 18 November 2010

Keywords:
Perovskite
Oxygen reduction
Oxygen evolution
Bi-functional electrode

ABSTRACT

Silver-modified $La_{0.6}Ca_{0.4}CoO_3$ composites for molecular oxygen reduction and evolution reaction are prepared by a chemical reduction process using N_2H_4 as the reducing agent at room temperature. The $La_{0.6}Ca_{0.4}CoO_3$ catalysts are modified with silver content that vary from 0.3 to 30 wt.% without damaging their microstructure. The electrochemical behavior of $La_{0.6}Ca_{0.4}CoO_3$ catalysts with different silver loadings is studied on classical bilayer gas diffusion electrodes. The electrocatalytic properties of these composites are evaluated by polarization curves and electrochemical impedance spectroscopy in alkaline electrolyte. The silver loading is found to have a significant impact on the electrode performances, which facilitate or block the electrochemical processes of the gas diffusion electrodes. The binary catalyst electrodes exhibit higher electrocatalytic activities than that of the electrodes with only $La_{0.6}Ca_{0.4}CoO_3$ as the catalyst. In this paper, the best performance was achieved when the silver loading was 3.0 wt.%.

1. Introduction

It's generally accepted by the current scientific community that oxygen reduction (ORR) and evolution (OER) in alkaline medium are critical electrochemical reactions in many energy storage applications. For example, in rechargeable metal–air batteries [1,2] and air–metal hydride [3], the oxygen reduction and generation reactions are of irreversibility which cause efficiency losses and lifetime problems for their catalysts and support materials. For accelerating electrochemical reactions, efficient bifunctional electrocatalysts turn to be indispensable. Recently, selection of electrocatalysts and the construction principle of bifunctional oxygen-air electrodes have been presented in some literatures [4–6]. Gas diffusion electrodes (GDEs) are prerequisites for many industrial devices [1–3,7] and usually used to screen suitable electrocatalysts.

Perovskite oxides, which have the general formula ABO_3, have been investigated extensively for their bifunctional catalytic abilities in alkaline electrolytes [8,9]. Their properties can be greatly changed by partially replacing A and B cations with other metals. Generally speaking, A-site substitution mainly affects the ability of sorbed oxygen, whereas B-site substitution influences the activity of sorbed oxygen [10,11]. Therefore, different perovskite type oxides with various replacements have been conducted by several groups as bifunctional catalysts [12–14]. Perovskite type oxides of the composition $La_{1-x}Ca_xMO_3$ (M = Ni, Mn, Co) have attracted considerable attention because of their reasonable electrocatalytic activities and corrosion resistance [15,16]. Among these candidate materials, $La_{0.6}Ca_{0.4}CoO_3$ can be found in many demonstration batteries and potentially replace noble metals in alkaline medium [1,17,18], so it is considered to be the most promising bifunctional catalyst [19–22]. However, perovskites normally have rather low conductivity and relatively poor catalytic activity. In order to solve these problems in real electrode systems, an addition of carbonaceous materials or other active materials is required. Previously, Wang et al. [23] mixed $La_{0.6}Ca_{0.4}CoO_3$ with some metal oxides (MnO_2, CaO) as electrocatalysts for GDEs, and found that the mixed catalyst was a much better choice for the air-electrode of metal–air battery. To date, Chang et al. [24–26] have successfully adulterated $La_{0.6}Ca_{0.4}CoO_3$ with iridium by three different preparation methods and observed that the doping of iridium in the perovskite structure of $La_{0.6}Ca_{0.4}CoO_3$ significantly enhanced its bifunctional abilities in alkaline medium.

Another method to improve the GDEs performance is to modify their catalysts with noble metals [27–31]. Owing to the high price of noble catalysts such as Ru, Rh, Ir, Pt and Pd, silver has gained notable attention. The focus has shifted from mono-catalyst to binary catalysts that combine two components to obtain a synergic effect [32–34]. It is expected that modifying catalysts with silver would result in an improvement in electrochemical performance of the GDEs. Additionally, the high activity of silver for oxygen reduction and evolution [3,35,36] probably have additional benefit to catalysts. Therefore, silver modification may be a practical way to increase the catalytic activity of $La_{0.6}Ca_{0.4}CoO_3$ for GDEs.

* Corresponding author. Tel.: +86 731 8887 9850; fax: +86 731 8887 9850.
E-mail address: huangkelong@163.com (K. Huang).

0378-7753/$ – see front matter © 2010 Elsevier B.V. All rights reserved.
doi:10.1016/j.jpowsour.2010.11.056

In this paper, to obtain a relatively more efficient bifunctional catalyst, different silver-loading modified $La_{0.6}Ca_{0.4}CoO_3$ electrocatalysts were synthesized by chemical reduction method. This technique allows for the preparation of modified $La_{0.6}Ca_{0.4}CoO_3$ catalyst with silver content varying from 0.3 to 30 wt.% without destruction to the catalyst microstructure and their bifunctional catalytic abilities in alkaline electrolyte using carbon black (Vulcan XC-72R) as the catalyst support were investigated. It was observed that the addition of silver significantly influenced the GDEs performance.

2. Experimental

2.1. Synthesis of catalyst powders and characterization

The catalyst $La_{0.6}Ca_{0.4}CoO_3$ powder was synthesized by an amorphous citrate precursor (ACP) method [37,19,38]. $La(NO_3)_3{\cdot}6H_2O$, $Ca(NO_3)_2{\cdot}4H_2O$, $Co(NO_3)_3{\cdot}6H_2O$ and citric acid were used as reagents. An aqueous solution of citric acid with a 10% excess over the number of ionic equivalents of cations was prepared. The aqueous solutions of the metal nitrates were added to that of citric acid, and they were agitated for 15 min. The resulting solution was concentrated by slowly evaporating water under vacuum in a rotavapor at 75 °C until a gel was obtained. This gel was dried in an oven, slowly increasing the temperature to 200 °C and maintaining this temperature overnight, to produce a solid amorphous citrate precursor. The precursor was milled and then calcined in air at 650 °C for 4 h. The resulted powder was then cooled by icy water.

In order to modify the $La_{0.6}Ca_{0.4}CoO_3$ powder with silver, chemical reduction process was adopted. $AgNO_3$ solution (0.01 mol L^{-1} for the $La_{0.6}Ca_{0.4}CoO_3$–0.3 wt.%Ag; 0.1 mol L^{-1} for the preparation of $La_{0.6}Ca_{0.4}CoO_3$–3 wt.%Ag and 1 mol L^{-1} for the preparation of $La_{0.6}Ca_{0.4}CoO_3$–30 wt.%Ag) was dropped (by a suction pipette with an accuracy of ±0.01 mL) and soaked into the $La_{0.6}Ca_{0.4}CoO_3$ catalyst, and then heated to evaporate the water. Silver loading was controlled through the dropped volume of $AgNO_3$ solution. When the desired silver loading was reached, necessary amount of N_2H_4 solution (1, 0.1 or 0.01 mol L^{-1}) was introduced as the reducing agent to initiate the Ag reduction reaction. Once the reaction was completed, the catalysts were heated at 80 °C over a hotplate to evaporate the water. Finally, the resulting products were milled and then calcined at 650 °C to stabilize the silver within the $La_{0.6}Ca_{0.4}CoO_3$ catalysts. Three kinds of $La_{0.6}Ca_{0.4}CoO_3$ oxide catalysts with 0.3, 3.0 and 30 wt.% of Ag were prepared and labeled as LCCO–0.003Ag, LCCO–0.03Ag and LCCO–0.3Ag, respectively.

Phase identifications of the synthesized powders were conducted by a MXPAHF X-ray diffractometer from 20° to 80° with a Cu Kα of 1.54056 Å. Both the morphologies and energy dispersive X-ray spectroscopy (EDS) of the silver-modified $La_{0.6}Ca_{0.4}CoO_3$ particles were observed by a JSM-SEM 6360.

2.2. Electrode preparation and electrochemical measurement

The manufacturing process for the electrodes is described as below. To prepare the semi-hydrophobic catalytic layer of the GDE, 25 wt.% catalyst powder and 50 wt.% carbon black (Vulcan XC-72R) were ball-milled in excess 2-propanol/H_2O (1:1) for 30 min, and then 25 wt.% diluted polytetrafluorethylene suspension (10 wt.% PTFE in H_2O) and proper quantities of acetone were added to the catalyst/Vulcan XC-72R mixture. In the presence of acetone, a very homogeneous dispersion of Teflon on a substrate was observed. This mixture was blended for 30 min with ultrasonic agitation and then dried at 80 °C to give a dough-like paste, which was finally rolled into a thin layer of about 200 μm thickness and the catalyst loading was approximately kept at 2.0 mg cm^{-2}. A hydrophobic gas diffusion layer containing only acetylene black and PTFE with weight ratios of 7:3 was prepared by the same process. The catalytic layer and a gas diffusion layer were finally rolled together with a stainless steel mesh current collector. The assembly was then dried and sintered for 30 min at 340 °C and 15 MPa.

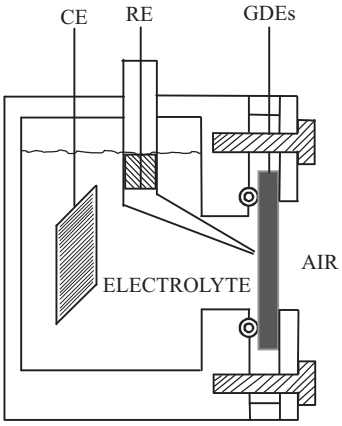

Fig. 1. Schematic diagram of the plexi-glass cell used for electrochemical measurements.

The GDEs were characterized with a three-electrode configuration as shown in Fig. 1. An area of 1 cm^2 on the backside of the GDE was exposed to ambient air during measurements. A bright platinum (2 cm^2) foil and an Hg/HgO/6 mol L^{-1} KOH electrode were used as counter and reference electrodes, respectively. The electrolyte was 6 mol L^{-1} KOH aqueous solution under air atmosphere and maintained at 25 °C. The half-cell had been rested for 48 h to assure that the electrolyte had sufficient time to penetrate into the structure of the active layer. In order to obtain steady polarization curves, galvanostatic measurements were applied. Then all polarization curves were obtained until they were repeatable. Electrochemical performances were conducted by Parstat 2273. The *i*–*V* polarization curves were obtained under a scan rate of 0.5 mV s^{-1}. Galvanostatic profiles were measured at current densities of 50 and 100 mA cm^{-2} for 10 min. For electrochemical impedance spectroscopy (EIS) measurement, the applied frequency range was from 0.01 Hz to 100 kHz with signal amplitude of 5 mV. The overall impedance data was fitted by a complex non-linear least squares fitting program in Z-view 2.0 software. None of

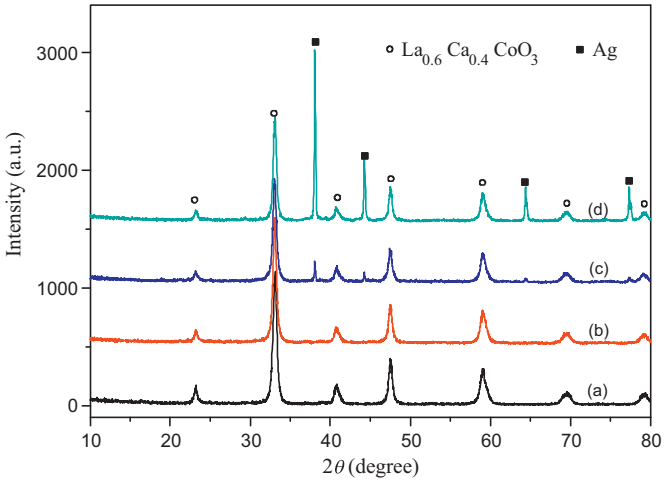

Fig. 2. XRD patterns of LCCO–0.003Ag (b), LCCO–0.03Ag (c) and LCCO–0.3Ag (d) catalysts fired at 650 °C together with the ACP-derived $La_{0.6}Ca_{0.4}CoO_3$ for comparison (a).

the potential measurements in this study were compensated for IR-drops.

In the lifetime determination, the GDEs experienced repeating sequences of oxygen reduction (0.5 h), resting (1 h), oxygen evolution (0.5 h), and resting (1 h) at 50 mA cm^{-2}. In order to test the stability of the modified-silver after the long-term cycle test, the silver contents of the electrolytes were analyzed using an inductively coupled plasma (ICP) spectrometer (Optima5300DV, Perkin Elmer).

3. Results and discussion

Fig. 2 presents the XRD patterns of the bifunctional catalysts with various silver loadings fired at 650 °C and the ACP-derived $La_{0.6}Ca_{0.4}CoO_3$ for comparison. The XRD result of the ACP-derived powders exhibited a pure perovskite $La_{0.6}Ca_{0.4}CoO_3$ phase, without any unwanted oxides, which agreed perfectly with the JCPDS standard data (36-1389). This suggested that the precursor calcinated at 650 °C in air for 4 h was sufficient to be decomposed, forming the desirable perovskite phase. Since the calcining temperature of the perovskite catalyst could also have a significant effect on the electrode performance [17], a fixed temperature of 650 °C was applied for preparing the $La_{0.6}Ca_{0.4}CoO_3$ catalyst throughout this investigation. After the modification of the $La_{0.6}Ca_{0.4}CoO_3$ with silver, all of the diffraction peaks in the samples could be indexed well based on the cubic perovskite phase of $La_{0.6}Ca_{0.4}CoO_3$. But, there was no Ag or Ag_2O phase detected when the silver loading was 0.3 wt.%. The characteristic diffraction peaks of Ag started to appear when the silver loading was more than 3 wt.%. The relative intensity of the diffraction peaks for silver to $La_{0.6}Ca_{0.4}CoO_3$ strengthened with the silver loading increased, indicating that the $La_{0.6}Ca_{0.4}CoO_3$ catalyst surface was successfully covered by Ag particle.

Fig. 3 shows the SEM images of the ACP-derived $La_{0.6}Ca_{0.4}CoO_3$ powders and silver-modified $La_{0.6}Ca_{0.4}CoO_3$ catalysts with various Ag loadings fired at 650 °C, together with the EDS spectra of the particles in the selected regions. As shown in Fig. 3(a) and (b), the ACP-derived $La_{0.6}Ca_{0.4}CoO_3$ powder exhibited particles aggregated in platelet shape. And no Ag grains could be clearly observed when

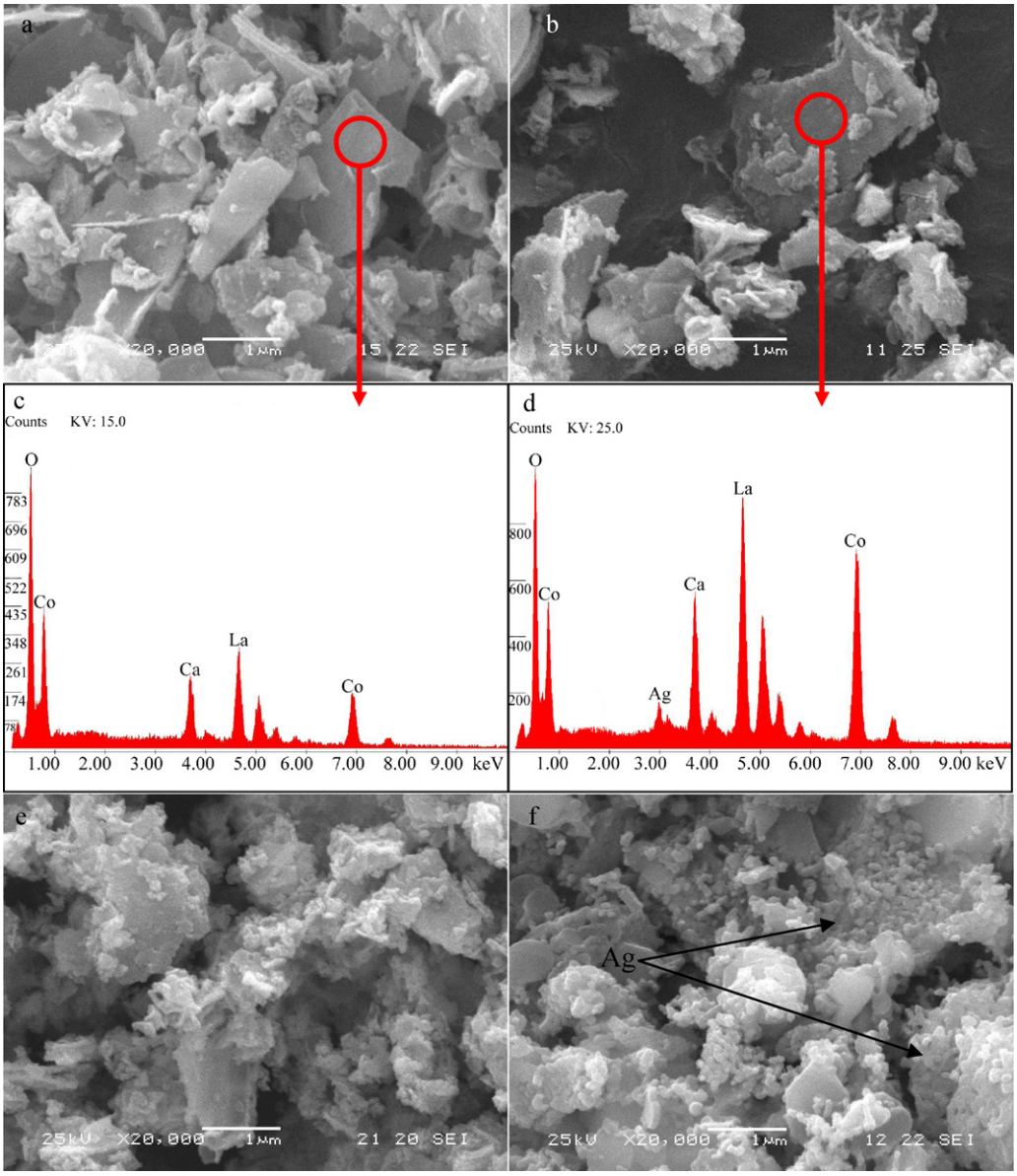

Fig. 3. SEM images of the ACP-derived $La_{0.6}Ca_{0.4}CoO_3$ powders (a) and silver-modified $La_{0.6}Ca_{0.4}CoO_3$ catalysts fired at 650 °C with the Ag loading of 0.3 wt.% (b), 3.0 wt.% (c), 30 wt.%; the EDS spectra collected onto the circular zones of images (a) and (b) for comparison.

the Ag loading was less than 3 wt.% while EDS did detect the silver element (Fig. 3(d)), which suggested that the Ag was very fine in nature and coating over the surfaces of the $La_{0.6}Ca_{0.4}CoO_3$ grains [42]. With the Ag loading further increasing, some coarse particles with round shape appeared which were proved to be the silvers from SEM (Fig. 3(f)). When the Ag loading reached 30 wt.%, the Ag particles became agglomerated and most of the $La_{0.6}Ca_{0.4}CoO_3$ catalyst surface were covered by silver particles. Since the silver coverage of the $La_{0.6}Ca_{0.4}CoO_3$ was closely related with the oxygen adsorption as well as the electronic conduction of the catalyst, a significant impact by the silver loadings on the catalytic activity could be expected.

Fig. 4(a) shows the oxygen reduction *i–V* curves for non-catalyzed GDE with a pure Vulcan XC-72R, catalyzed GDEs with LCCO–0.003Ag, LCCO–0.03Ag, and LCCO–0.3Ag in the catalyst layer. Catalyzed GDEs with $La_{0.6}Ca_{0.4}CoO_3$ is also presented as the reference. The profiles demonstrated typical *i–V* polarizations in which the potential values started around −50 mV and decreased gradually with increasing current densities. It was determined that all catalyzed GDEs exhibited considerable electrocatalytic enhancement over that of non-catalyzed GDE. The non-catalyzed GDE showed negligible catalytic behaviors. As mentioned by Hermann [39], oxygen reduction took place mainly on the carbon, where H_2O_2 was formed. The catalysts led to more rapid decomposition of the H_2O_2 and a subsequent decrease of overpotential for ORR. Among these catalyzed GDEs, LCCO–0.03Ag exhibited the highest performance, presenting −245 mV and −341 mV at 100 and 200 mA cm^{-2}, respectively. In contrast, $La_{0.6}Ca_{0.4}CoO_3$ delivered −306 mV and −407 mV at identical current densities. The results clearly indicated that the silver-modified $La_{0.6}Ca_{0.4}CoO_3$ binary catalysts presented significant improvement in ORR capability. The increased activity might be explained by a synergic effect of the silver modified $La_{0.6}Ca_{0.4}CoO_3$ catalyst in which silver and $La_{0.6}Ca_{0.4}CoO_3$ took part in different steps in the reaction mechanism for the oxygen reduction reaction. Nevertheless, with the further increasing of the silver, the catalytic ability of LCCO–0.3Ag conversely decreased. This was mainly because excessive silver that covered around the $La_{0.6}Ca_{0.4}CoO_3$ surface might block the path for electrolyte and gas to reach the $La_{0.6}Ca_{0.4}CoO_3$ surface and thus led to less active three phase boundary sites in the catalytic layer.

Fig. 4(b) shows the Tafel plots of the data in Fig. 5. Wang et al. [23] and Wu et al. [19] found that the Tafel curves were divided into two regions, which indicated that the catalytic activities of $La_{0.6}Ca_{0.4}CoO_3$ towards oxygen reduction were affected by two mechanisms involving mainly the intermediate two-electron reduction path into HO_2^- accompanied with a four-electron direct path reduction of O_2 into OH^-. As shown in Fig. 5, two Tafel zones were also observed for the reduction of oxygen. Thus, the mechanisms of oxygen reduction reaction on the binary catalysts were considered to be similar to that on the perovskites. At any given potential, the electrodes with different catalyst gave different polarization behavior and suggest different electrocatalytic activity. Among these samples, LCCO–0.03Ag exhibited the highest performance which was in accord with Fig. 4(a).

The oxygen evolution *i–V* curves for the non-catalyzed GDE, as well as GDEs catalyzed by $La_{0.6}Ca_{0.4}CoO_3$, LCCO–0.003Ag, LCCO–0.03Ag, and LCCO–0.3Ag are provided in Fig. 5. In oxygen evolution reaction, oxygen was produced and released from the GDEs. Generally, the oxygen evolution exhibited a much larger polarization loss compared to oxygen reduction at an identical current density [5,40]. As shown in Fig. 5, the voltage started at 0.5 V vs. Hg/HgO and increased rapidly with increasing current densities. Apparently, the non-catalyzed GDE presented the poorest oxygen evolution performance. In contrast, all catalyzed GDEs showed great improvement in OER capability. Furthermore, the GDEs catalyzed by silver-modified $La_{0.6}Ca_{0.4}CoO_3$ binary catalysts exhibited a smaller polarization than the one that without silver. The GDEs catalyzed by LCCO–0.03Ag demonstrated impressive catalytic performances, showing voltages of 0.68 V and 0.75 V (vs.

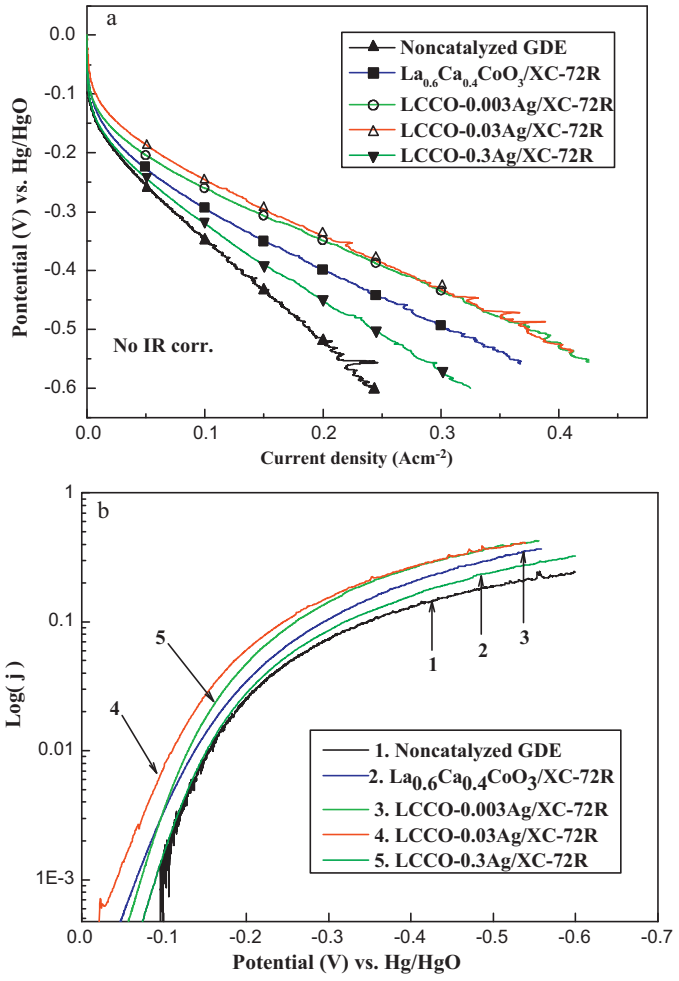

Fig. 4. (a) Cathodic polarization curves of non-catalyzed GDE and catalyzed GDEs with $La_{0.6}Ca_{0.4}CoO_3$/XC-72R, LCCO–0.003Ag/XC-72R, LCCO–0.03Ag/XC-72R, and LCCO–0.3Ag/XC-72R. (b) Tafel plots of *i–V* data in (a).

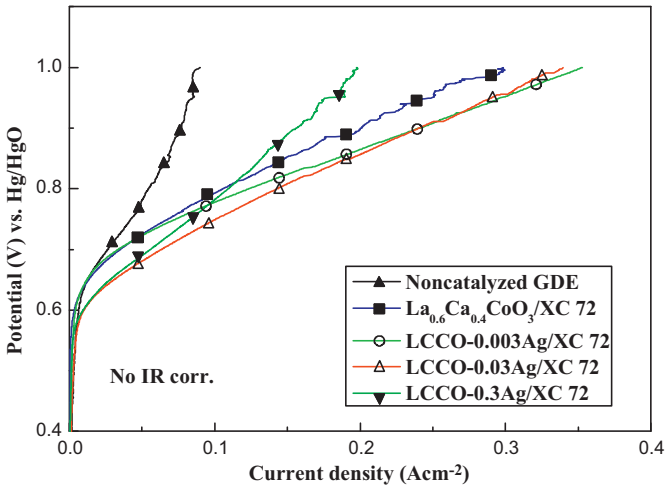

Fig. 5. Anodic polarization curves of noncatalyzed GDE and catalyzed GDEs with $La_{0.6}Ca_{0.4}CoO_3$/XC-72, LCCO–0.003Ag/XC-72, LCCO–0.03Ag/XC-72, and LCCO–0.3Ag/XC 72, respectively.

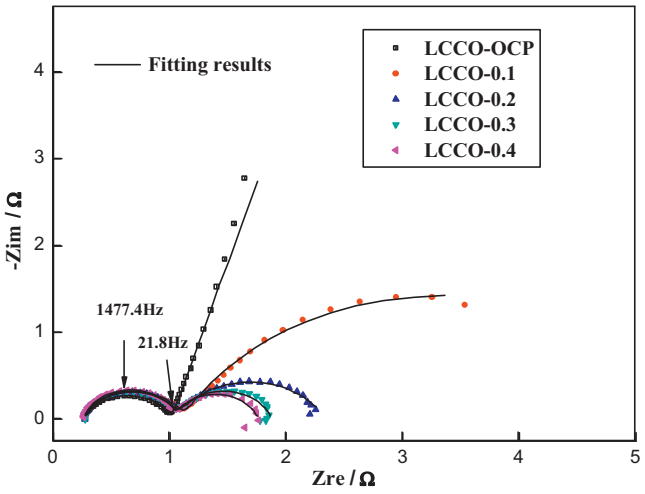

Fig. 6. Impedance spectra of the GDEs catalyzed by LCCO recorded at cathodic potentials of −100, −200, −300, −400 mV (vs. OCP) and the fitting results.

Hg/HgO) at 50 mA cm^{-2} and 100 mA cm^{-2}, respectively. This might be ascribed to the rapid oxygen adsorption and desorption when the silver particles were introduced [38,39,41]. Compared with the LCCO–0.03Ag electrode, the current on the LCCO–0.3Ag electrode had little difference at low overpotentials but deteriorates rapidly at high overpotentials. The difference in the polarization features were also related to the less active catalytic sites when the silver loadings increased. The results from the *i*–*V* measurements for oxygen reduction and evolution were encouraging. With the introduction of silver particles on the $La_{0.6}Ca_{0.4}CoO_3$ surface, the bifunctional catalytic abilities for oxygen evolution and reduction were obviously improved.

In order to gain additional supporting evidence, the EIS characteristic of the electrode catalyzed by LCCO has been investigated and the corresponding Nyquist plots at the different cathodic potentials and the fitting results are shown in Fig. 6. Two semicircles were observed in the frequency range from 100 kHz to 100 mHz. The Nyquist plots displayed a high frequency loop and a low frequency potential-dependent loop as described in Ref. [42]. The size of the first one in the high frequency region remained virtually unchanged with increasing the over potential, which was ascribed to distributed resistances inside the porous structure. The second one, which was expected for kinetic impedance of ORR, decreased with increasing the overpotential. The spectra were fitted with an equivalent circuit shown in Fig. 7. The parameters were obtained and listed in Table 1. Compared R_1 with R_2 in Table 1, at

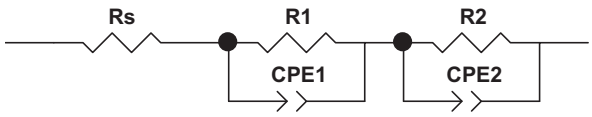

Fig. 7. Schematic representation of the equivalent circuit for the EIS of the bifunctional air electrode.

low overpotentials, R_2 was bigger than R_1, inferring that the reaction rate is determined by the kinetic of oxygen reduction on the catalyst and carbon support. While at high overpotentials, R_1 and R_2 were comparable. Thus, both the ohmic process within the porous structure and the kinetic of oxygen reduction on the catalyst and carbon support determined the reaction rate.

The resistance R_s represented the sum of electrolyte resistance and contact resistances. It was the high frequency intercept with the real axis in the Nyquist plot. The two semi-circles were described by a series of two parallel RC elements, whereby the capacitances were replaced by constant phase elements. CPE_1 and CPE_2 represented the double-layer capacitance distributed between the ohmic and Faradic processes. The high frequency resistance R_1 accounted for electrode intrinsic resistance and the low frequency resistance R_2 was related to charge transfer processes at the catalyst surface and reacting species diffusion through the thin film.

The Nyquist plots of the electrodes with different catalyst for ORR obtained at potentials of −200 mV (vs. OCP) are shown in Fig. 8. The spectra of Fig. 8 were fitted with aforesaid equivalent circuit (Fig. 7). The parameters were obtained by analyzing the data in Fig. 8 and listed in Table 2. R_1 was decreasing with the increase of silver loading, whereas R_2 decreased initially and then increased with the increase of silver loading. The corresponding results confirmed that the introduction of silver on the catalyst surface decreases intrinsic and kinetic impedance. In Fig. 8, the diameter of low-frequency loops had a minimum value when the silver loadings was 3 wt.%. This implied that this electrode had the highest electrocatalytic activity.

Galvanostatic measurements of the GDEs catalyzed with LCCO–0.03Ag for the oxygen reduction reaction were performed for 10 min at current densities of 50 and 100 mA cm^{-2}, respectively. The results were shown in Fig. 9, along with those of the GDEs catalyzed with $La_{0.6}Ca_{0.4}CoO_3$ for comparison. For the two samples, the voltage readings agreed well with the results of *i*–*V* polarization curves (shown in Fig. 4). The voltage plateaus were rather flat, indicating that the catalytic performances of $La_{0.6}Ca_{0.4}CoO_3$ and LCCO–0.03Ag were stable and sustainable. In addition, the voltage readings from LCCO–0.03Ag were consistently higher than those of $La_{0.6}Ca_{0.4}CoO_3$ for both current densities. Fig. 10 presents the oxy-

Table 1
The corresponding fitting parameters of Fig. 6 for ORR on the GDEs with LCCO at different cathodic potentials.

Sample	R_s/Ω	R_1/Ω	CPE_1-T/F	CPE_1-P	R_2/Ω	CPE_2-T/F	CPE_2
LCCO-OCP	0.27	0.80	1.5×10^{-3}	0.79	5.6×10^{13}	0.52	0.83
LCC-0.1V	0.27	0.84	9.3×10^{-4}	0.81	4.5	0.31	0.71
LCC-0.2V	0.27	0.84	6.7×10^{-4}	0.84	1.26	0.15	0.75
LCC-0.3V	0.27	0.84	5.5×10^{-4}	0.84	0.81	0.1	0.84
LCC-0.4V	0.27	0.84	4.0×10^{-4}	0.85	0.71	0.095	0.86

Table 2
The corresponding fitting parameters of Fig. 8 for ORR on GDEs.

Composition of catalyst	R_s/Ω	R_1/Ω	CPE_1-T/F	CPE_1-P	R_2/Ω	CPE_2-T/F	CPE_2-P
$La_{0.6}Ca_{0.4}CoO_3$	0.27	0.84	6.7×10^{-4}	0.84	1.26	0.15	0.75
LCC–0.003Ag	0.29	0.18	5.3×10^{-4}	0.89	1.14	0.045	0.93
LCC–0.03Ag	0.29	0.15	0.015	0.76	0.67	0.043	0.98
LCC–0.3Ag	0.29	0.13	0.26	0.46	1.47	0.025	0.94

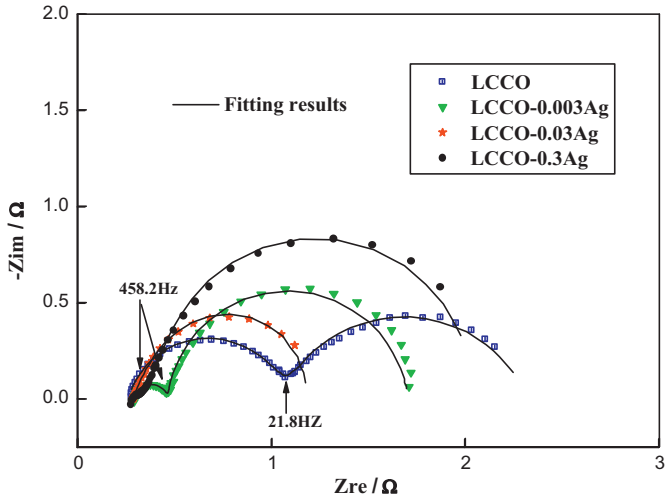

Fig. 8. Impedance spectra at a potential of −200 mV (vs. OCP) for $La_{0.6}Ca_{0.4}CoO_3$ and binary catalysts electrodes and the fitting results.

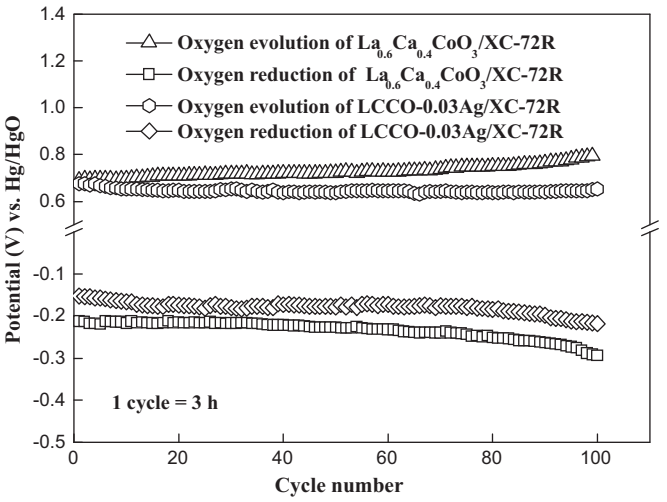

Fig. 11. The cycle life performance of LCCO–0.03Ag/XC-72R-catalyzed GDE and $La_{0.6}Ca_{0.4}CoO_3$/XC-72R-catalyzed GDE for comparison with the current density at 50 mA cm^{-2}.

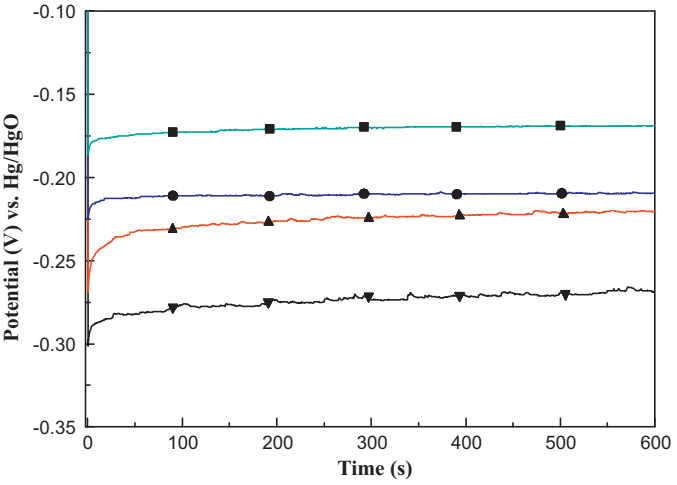

Fig. 9. Oxygen reduction galvanostatic curves for LCCO–0.03Ag at current densities of 50 mA cm^{-2} (■) and 100 mA cm^{-2} (▲), as well as $La_{0.6}Ca_{0.4}CoO_3$ at current densities of 50 mA cm^{-2} (●) and 100 mA cm^{-2} (▼).

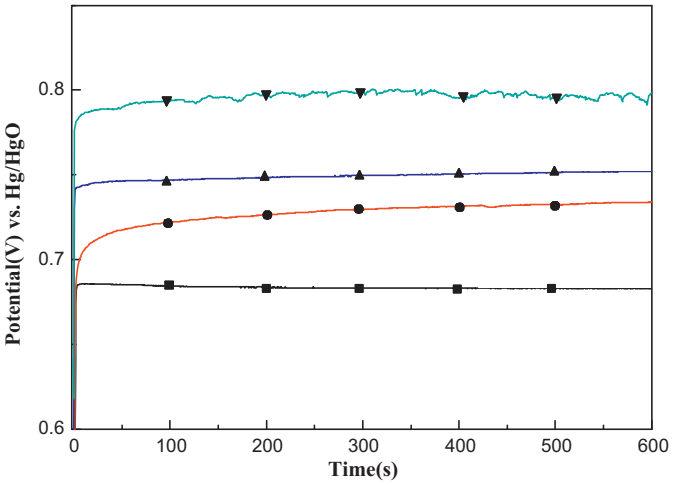

Fig. 10. Oxygen evolution galvanostatic curve for LCCO–0.03Ag at current densities of 50 mA cm^{-2} (■) and 100 mA cm^{-2} (▲), as well as $La_{0.6}Ca_{0.4}CoO_3$ at current densities of 50 mA cm^{-2} (●) and 100 mA cm^{-2}(▼).

gen evolution galvanostatic profiles for the GDEs catalyzed with $La_{0.6}Ca_{0.4}CoO_3$ and LCCO–0.03Ag at current densities of 50 and 100 mA cm^{-2} for 10 min. Likewise, the voltage readings were consistent with *i*–*V* polarization curves (shown in Fig. 5), and their responses were relatively steady.

To fairly compare the bi-functional ability and the stability of LCCO–0.03Ag/XC-72R with those of $La_{0.6}Ca_{0.4}CoO_3$/XC-72R, the catalyzed GDEs were subjected to 100 cycles of oxygen reduction and evolution. The results are shown in Fig. 11. Compared with $La_{0.6}Ca_{0.4}CoO_3$/XC-72R, LCCO–0.03Ag/XC exhibited higher catalytic ability and stability. For LCCO–0.03Ag/XC-72R-catalyzed GDE, the voltages slightly went down initially, but moved up steadily after 10 cycles in the oxygen evolution reactions. Similarly, the voltages in the oxygen reduction reactions decreased upon cycling and then kept steady after 10 cycles. This phenomenon was ascribed to the fact that it would cost time for the electrolyte to penetrate into the structure of the active layer to form the three-phase boundary. From the 10th cycle to the 80th cycle, the voltages in the oxygen reduction and evolution reactions were very stable. After the 80th cycle, the slopes of the voltage declines were 3.2 mV cycle^{-1} in the oxygen evolution reaction and 1.2 mV cycle^{-1} in the oxygen reduction reaction. Since the backside of the GDE

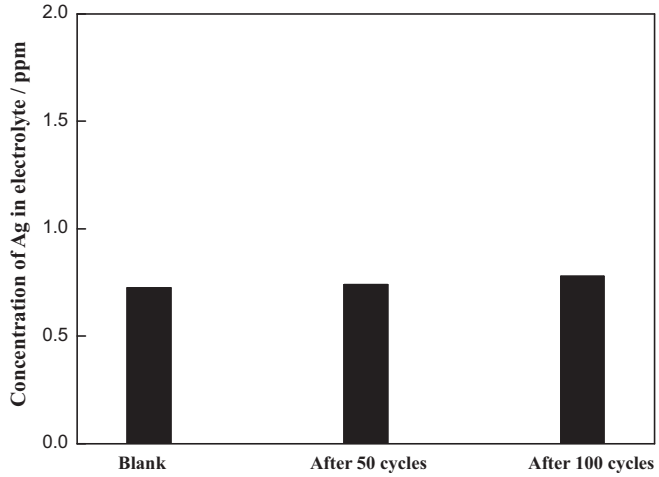

Fig. 12. Concentration of Ag ions dissolved from the active layer of LCC–0.03Ag/XC-72R-catalyzed GDE after 50 cycles and 100 cycles at the current density of 50 mA cm^{-2}.

was exposed to ambient air during measurements, the carbonation-induced electrode might be damage, which was possibly resulting in the performance degradation of the electrode. In addition, it is recognized that oxidation of the carbon supports during the oxygen evolution reaction can lead to the gradual loss of catalytic abilities [43,44].

In order to understand the stability of the modified-silver, the content of Ag ions in the electrolytes were measured by ICP after different cycles. The amount of Ag ions dissolved from the active layer in the electrolyte after different cycles was compared in Fig. 12. As shown in chart, the content of Ag ions slightly increased with cycling (from 0.725 ppm in the fresh electrolyte to 0.739 ppm after 50 cycles and 0.778 ppm after 100 cycles compared with 0.725 ppm in new electrolyte). This result illuminated that the modified-silver was relative stable during long-term cycles.

Obviously, the electrocatalytic performance of LCCO–0.03Ag surpassed that of $La_{0.6}Ca_{0.4}CoO_3$ for ORR and OER, which further confirmed that the modification of $La_{0.6}Ca_{0.4}CoO_3$ with silver resulted in a remarkable improvement in bifunctional abilities.

4. Conclusions

Silver-modified $La_{0.6}Ca_{0.4}CoO_3$ catalysts were prepared by the chemical reduction method using N_2H_2 as the reducing agent. Based on XRD and SEM results, the Ag particles were dispersed on the surface of $La_{0.6}Ca_{0.4}CoO_3$. Compared with the electrodes only catalyzed by $La_{0.6}Ca_{0.4}CoO_3$, the silver-modification $La_{0.6}Ca_{0.4}CoO_3$ binary catalyst electrodes demonstrated improved bifunctional catalytic abilities in *i–V* polarizations. Similar behaviors were observed by galvanostatic measurements for oxygen reduction and evolution reactions. The best performance was observed on the electrode which was catalyzed by LCCO–0.03Ag. However, excessive Ag loading reduced the active sites and led to the slower diffusion process for ORR and OER. Additionally, the EIS analysis indicates that the introduction of silver particles on the $La_{0.6}Ca_{0.4}CoO_3$ surface not only enhanced the electronic conductivity, but also increased the ORR kinetics. These exciting results provided conclusive evidence that the modification of silver on the surface of perovskite $La_{0.6}Ca_{0.4}CoO_3$ significantly enhanced its bifunctional abilities in the alkaline medium.

Acknowledgement

This work was financially supported by Chinese 863 program (no. 2008AA031205).

References

[1] S. Müller, O. Haas, J. Appl. Electrochem. 28 (1998) 305.
[2] A. Weidenkaff, S.G. Ebbinghaus, T. Lippert, Chem. Mater. 14 (2002) 1797.
[3] M.V. Anantha, K. Manimarana, I.A. Raj, N. Sureka, Int. J. Hydrogen Energy 32 (2007) 4267.
[4] L. Jörissen, J. Power Sources 155 (2006) 23.
[5] V. Nikolova, P. Iliev, K. Petrov, T. Vitanov, E. Zhecheva, R. Stoyanova, I. Valov, D. Stoychev, J. Power Sources 185 (2008) 727.
[6] S. Müller, K. Striebel, O. Haas, Electrochim. Acta 39 (1994) 1661.
[7] H.Y. Jung, S. Park, B.N. Popov, J. Power Sources 191 (2009) 357.
[8] M. Bursell, M. Pirjamali, Y. Kiros, Electrochim. Acta 47 (2002) 1651.
[9] V. Neburchilov, H.J. Wang, J.J. Martin, W. Qu, J. Power Sources 195 (2010) 1271.
[10] H.M. Zhang, Y. Shimizu, Y. Teraoka, N. Miura, N. Yamazoe, J. Catal. 121 (1990) 432.
[11] H. Tanaka, M. Misono, Curr. Opin. Solid State Mater. Sci. 5 (2001) 381.
[12] L. Swette, N. Kackley, S.A. McCatty, J. Power Sources 36 (1991) 323.
[13] A.M. Kannan, A.K. Shukla, S. Sathyanarayana, J. Power Sources 25 (1989) 141.
[14] L. Swette, N. Kackley, J. Power Sources 29 (1990) 423.
[15] Y. Shimizu, K. Uemura, H. Matsuda, N. Miura, N. Yamazoe, J. Electrochem. Soc. 137 (1990) 3430.
[16] Y. Shimizu, H. Matsuda, N. Miura, N. Yamazoe, Chem. Lett. 21 (1992) 1033.
[17] C.K. Lee, K.A. Striebel, F.R. Mclarnon, E.J. Cairns, J. Electrochem. Soc. 144 (1997) 3801.
[18] S. Müller, F. Holzer, O. Haas, J. Appl. Electrochem. 28 (1998) 895.
[19] N.L. Wu, W.R. Liu, S.J. Su, Electrochim. Acta 48 (2003) 1567.
[20] D. Chartouni, N. Kuriyama, T. Kiyobayashi, J. Chen, J. Alloys Compd. 330-332 (2002) 766.
[21] N.A. Merino, B.P. Barbero, P. Eloy, L.E. Cadús, Appl. Surf. Sci. 253 (2006) 1489.
[22] A. Kahoul, A. Hammouche, G. Poillerat, R.W. De Doncker, Catal. Today 89 (2004) 287.
[23] X.Y. Wang, P.J. Sebastian, M.A. Smit, H.P. Yang, S.A. Gamboa, J. Power Sources 124 (2003) 278.
[24] Y.M. Chang, P.W. Wu, C.Y. Wu, Electrochem Solid State Lett. 11 (2008) B47.
[25] Y.M. Chang, Y.C. Hsien, P.W. Wu, C.H. Lai, T.Y. Chang, Mater. Lett. 62 (2008) 4220.
[26] Y.M. Chang, P.W. Wu, C.Y. Wu, Y.C. Hsien, J. Power Sources 189 (2009) 1003.
[27] S.P. Simner, M.D. Anderson, J.W. Templeton, J.W. Stevenson, J. Power Sources 168 (2007) 236.
[28] T. Kenjo, S. Osawa, K. Fujikawa, J. Electrochem. Soc. 138 (1991) 349.
[29] S.P. Simner, M.D. Anderson, J.E. Coleman, J.W. Stevenson, J. Power Sources 161 (2006) 115.
[30] K. Sasakia, K. Hosodaa, T.N. Lanb, K. Yasumotoc, S. Wang, M. Dokiyaa, Solid State Ionics 174 (2004) 97.
[31] J.D. Zhang, Y. Ji, H.B. Gao, T.M. He, J. Liu, J. Alloys Compd. 395 (2005) 322.
[32] G.Q. Zhang, X.G. Zhang, Y.G. Wang, Carbon 42 (2004) 3097.
[33] F.P. Hu, X.G. Zhang, F. Xiao, J.L. Zhang, Carbon 43 (2005) 2931.
[34] G.Q. Zhang, X.G. Zhang, Electrochim. Acta 49 (2004) 873.
[35] L. Carlsson, L. Öjefors, J. Electrochem. Soc. 127 (1980) 525.
[36] N. Wagner, M. Schulze, E. Gülzow, J. Power Sources 127 (2004) 264.
[37] N.A. Merino, B.P. Barbero, P. Grange, L.E. Cadús, J. Catal. 321 (2005) 232.
[38] W. Zhou, R. Ran, Z.P. Shao, R. Cai, W.Q. Jin, N.P. Xu, J. Ahn, Electrochim. Acta 53 (2008) 4370.
[39] V. Hermann, D. Dutriat, S. Müller, C. Comninellis, Electrochim. Acta 46 (2000) 365.
[40] M.D. Koninck, B. Marsan, Electrochim. Acta 53 (2008) 7012.
[41] J.H. Wang, M.L. Liu, M.C. Lin, Solid State Ionics 177 (2006) 939.
[42] H. Huang, W. Zhang, M. Li, Y. Gan, J. Chen, Y. Kuang, J. Colloid Interface Sci. 284 (2005) 593.
[43] M. Pirjamali, Y. Kiros, J. Power Sources 109 (2002) 446.
[44] T. Burchardt, J. Power Sources 135 (2004) 192.